Mold Slag Entrainment Mechanisms in Continuous Casting Molds

Entrainment is one of the main sources of inclusions in the final product, and so greatly harms clean steel production. By understanding the mechanisms that cause entrainment, the operating condition windows can be chosen to reduce defects. Nine mechanisms have been proposed over the last three decades. Previous investigations into each of these mechanisms are summarized. The quantitative models are combined to suggest best practices for clean steel production, but more work is needed to improve these predictions.

Authors

Lance C. Hibbeler
Department of Mechanical Science and Engineering, University of Illinois at Urbana–Champaign, Urbana, Ill., USA
lhibbel2@illinois.edu

Brian G. Thomas
professor, Department of Mechanical Science and Engineering, University of Illinois at Urbana–Champaign, Urbana, Ill., USA
bgthomas@illinois.edu

Mold slag (or mold flux) entrainment, also called emulsification, engulfment, entrapment or involvement, is characterized by mold powder being drawn into the molten steel pool inside a continuous casting mold. Mold slag entrainment can cause both surface and internal defects in the final product if the entrained droplets become trapped in the solidifying metal, which makes it a significant problem in the production of clean steel.

Slag entrainment has received much attention in the steel industry over the past three decades, resulting in several proposed mechanisms. Some of these mechanisms are relevant to other industrial processes involving fluid flow. The entrainment mechanisms reported in the literature fall into nine families: top surface-level fluctuations, meniscus freezing, vortexing, shear-layer instability, narrow-face spout impingement upon the top surface, argon bubble interactions, slag crawling down the submerged entry nozzle (SEN), instability of the top surface standing wave, and top surface balding. Most mechanisms suggest a critical condition for entrainment that can be used as a practical evaluation of models of fluid flow in a caster, and also can be used together to define a safe operating window to avoid inclusions in the final product.

Many studies are based on measurements from room-temperature physical models, usually employing water and silicon oil as surrogate fluids for the molten steel and slag. These physical models are unable to meet all of the relevant similarity criteria simultaneously, so their results are difficult to interpret quantitatively. Typically, the bulk fluid flow pattern and top surface profile of the caster are captured in the water model by matching the Froude number and ensuring that the Reynolds number is in the turbulent regime.[1] This requirement leaves the Weber number, mass density ratio, shear viscosity ratio and other similarity criteria unsatisfied with most choices of fluids, so important phenomena such as interfacial tension effects are not reproduced properly. Additionally, the surrogate liquid properties can be changed with additives, which usually affect multiple properties, e.g., an additive to change interfacial tension also may change the mass density, so it is difficult to isolate the individual contributions to the entrainment mechanisms. Any prediction of entrainment from a physical model must be interpreted skeptically since all of these phenomena inherently are important to entrainment.

The ever-advancing computer technology and computational fluid dynamics techniques have allowed numerical investigations of slag entrainment, though challenges related to turbulent and multiphase flows remain. The computational models discussed in this article include a variety of numerical techniques, turbulence models and simulated physics. Computational modeling presents many challenges, such as grid-dependent errors and missing physics, but allows for precise control of physical properties; if done properly, this technique offers the potential for better insight into the underlying physics than physical models.

The previous works on this subject all agree that mold slag entrainment depends on the physical properties of the materials involved (especially mass density ρ, dynamic shear viscosity μ, and interfacial tension between fluids A and B Γ_{AB}); the slag/powder layer thickness h_u; the flow system design (including SEN submergence depth h_{SEN}, SEN geometry and SEN port geometry); and the operating conditions (including casting speed V_C, strand/mold width w_{strand} and thickness t_{strand}, argon gas flowrate Q_{Ar}, and electromagnetic flow control).

Throughout this article, the subscript u refers to the upper fluid layer (melted mold powder or oil, etc.) and the subscript ℓ refers to the lower fluid layer (mold steel or water, etc.). Other symbols used in this article are the mass density ratio $r = \rho_u/\rho_\ell$, dynamic shear viscosity ratio $m = \mu_u/\mu_\ell$, velocity magnitudes V, flowrates Q and the acceleration due to gravity g. The immersion depth of the SEN h_{SEN} is defined as the vertical distance between the the average position of top surface and the top edges of the ports.

Entrainment Does Not Guarantee Inclusions

At the outset, it must be emphasized that entrainment is not detrimental to product quality unless the entrained particles become captured into the solidifying steel.

Studies have shown[2] that most slag droplets entrained into the molten steel are recaptured quickly back into the slag layer due to their buoyancy. A numerical study[3] showed that particles may or may not become captured in an approaching dendritic solidification front, depending on the particle diameter and composition, local crossflow velocity, steel composition and other parameters. Downward flow velocities may exacerbate entrapment by suspending the rising particles and slag-coated argon bubbles in front of the solidifying interface,[4] which may explain why single-roll patterns are found to produce more slag entrainment defects.[5] This model[3] has predicted that the flow pattern in the mold should deliver 70% of large (400 μm) particles to the slag layer, but less than 10% of small (10–40 μm) particles. The particle size produced by an entrainment mechanism, if known, is reported in this article for use with these entrapment models.

The capability of the liquid slag layer to absorb or reabsorb the inclusions that reach it depends greatly on the composition of the slag.[6,7] Dynamic models have been constructed for solid[8] and liquid[9] particles to determine if a particle will enter the slag layer; the tendency to absorb decreases with decreasing inclusion particle diameter, decreasing wettability between the slag and particles, increasing interfacial tension and increasing slag viscosity. However, as discussed in this article, the same properties that encourage inclusion removal often make entrainment more likely.

Top Surface Fluctuations

The early studies of slag entrainment focused on the high-frequency, localized fluctuations of the top surface, likely because they are measurable in the plant and strongly correlate with the number of inclusion particles measured in the final product. However, numerical modeling[10,11] has revealed how these fluctuations can entrain slag at the meniscus by exposing the dendritic solidification front at the top of the strand to the liquid slag and mold powder during a sudden drop in the liquid level. Figure 1 illustrates the sequence of events leading to entrainment by this mechanism. Although mold oscillation causes slight changes in the liquid level during each cycle, it is the transient changes in the flow pattern in the mold that cause the bigger-level fluctuations that result in slag-entrainment defects. If the level fluctuations are severe enough relative to the slag layer thickness, this mechanism can even entrain solid mold powder. However, "severe enough" has not yet been quantified for either solid or liquid particle entrainment by this mechanism. In addition to turbulence and mold oscillations, the top surface-level fluctuations can be caused by upstream flow control devices such as a slidegate[12] or stopper rod,[13] or shell bulging in secondary cooling.

Top surface fluctuations are associated with the turbulence of the liquid steel pool. The amplitude of the fluctuations increases with increasing casting speed,[14,15] increasing SEN bore diameter,[16] increasing SEN port size,[16] aiming the SEN port angles more upward,[15,16] more shallow SEN immersion depth,[15,17] and decreasing slab width.[15,18] Fluctuations also increase with increasing argon flowrate,[15,16,19] especially so with poor wettability between the argon and SEN refractory material,[19] but increasing the casting speed decreases the effect of the bubbles.[15] The effects of argon bubbles are discussed further in the section entitled, "Argon Bubble Interactions."

Figure 1

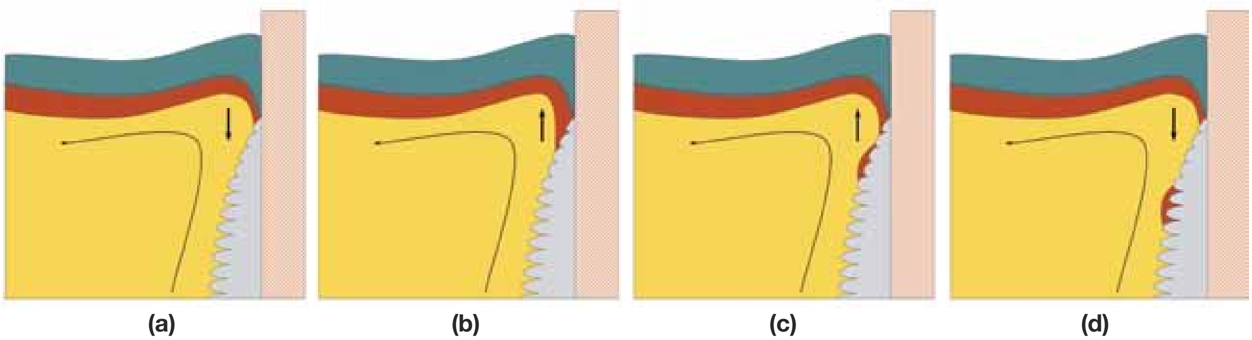

Entrainment by meniscus level fluctuation: start of level fluctuation (a); slag-shell contact (b); level rise and entrained slag (c); and end of level fluctuation (d).

The turbulence of the meniscus in water models has been observed, both by direct observation[20] and by measurements of turbulent kinetic energy,[21] to increase sharply with decreasing SEN immersion depth; the meniscus becomes quiet at sufficiently large immersion depths.[20–22] The fluctuations in a water model[23] were suppressed with the proper combination of SEN immersion depth, argon flowrate and SEN geometry, but all of these parameters depend on casting speed and mold width.

Fluctuations were observed in an actual caster[24] to have the same frequency and have about 70% of the amplitude of the applied mold oscillations. This percentange was observed to increase with casting speed,[24] but a water model study[22] showed that the fluctuation amplitude is independent of casting speed. The frequency of the fluctuations is the superposition of a low-frequency signal corresponding to the turbulent fluctuations of the SEN jet[22] and a high-frequency signal[22,25] corresponding perhaps to a sloshing frequency. The natural frequency for gravity wave sloshing can be amplified by improper slidegate dithering practice.[12] The low-frequency effects of the jet wandering in the molten steel pool[26,27] scale with the Strouhal number fh_{SEN}/V_C.[26] This jet wandering can produce transient surface velocities near 1 m/second.[26]

Single-roll flow patterns are more susceptible to defects via this mechanism, and combinations of flow-control variables that produce continuously unstable complex flow patterns are worse.[28] Electromagnetic forces offer another variable to control the flow pattern. Plant experiments using electromagnetic braking have reported decreases in level fluctuations and associated defects.[29] Other plant experiments have reported the use of traveling electromagnetic field stirring to control fluctuations and significantly reduce the number of defects.[14]

In double-roll flow patterns, many flow-related phenomena, including level fluctuations, strongly correlate with the strength of the flow up the narrowface, discussed further in the section entitled, "Upward Flow Impinging Upon the Top Surface." One characterization of the effect of SEN and mold geometry on the strength of flow up the narrowface is the "*F* Value,"[15] defined as:

$$F = \rho_\ell Q_{SEN} V_{coll} \frac{1 - \sin(\theta_{coll})}{4h_{coll}} \quad \text{(Eq. 1)}$$

where

Q_{SEN} is the flowrate through the SEN.

Figure 2

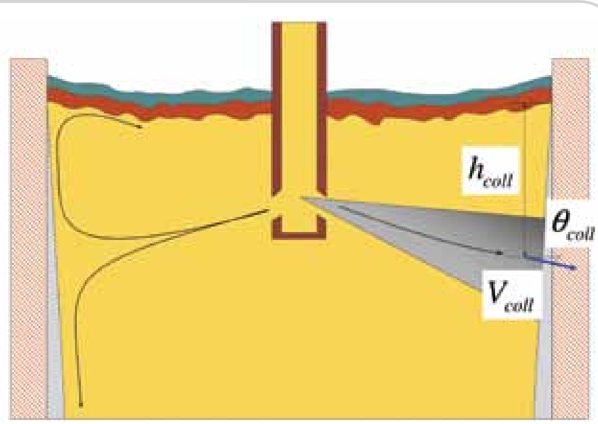

F value model description.

Figure 3

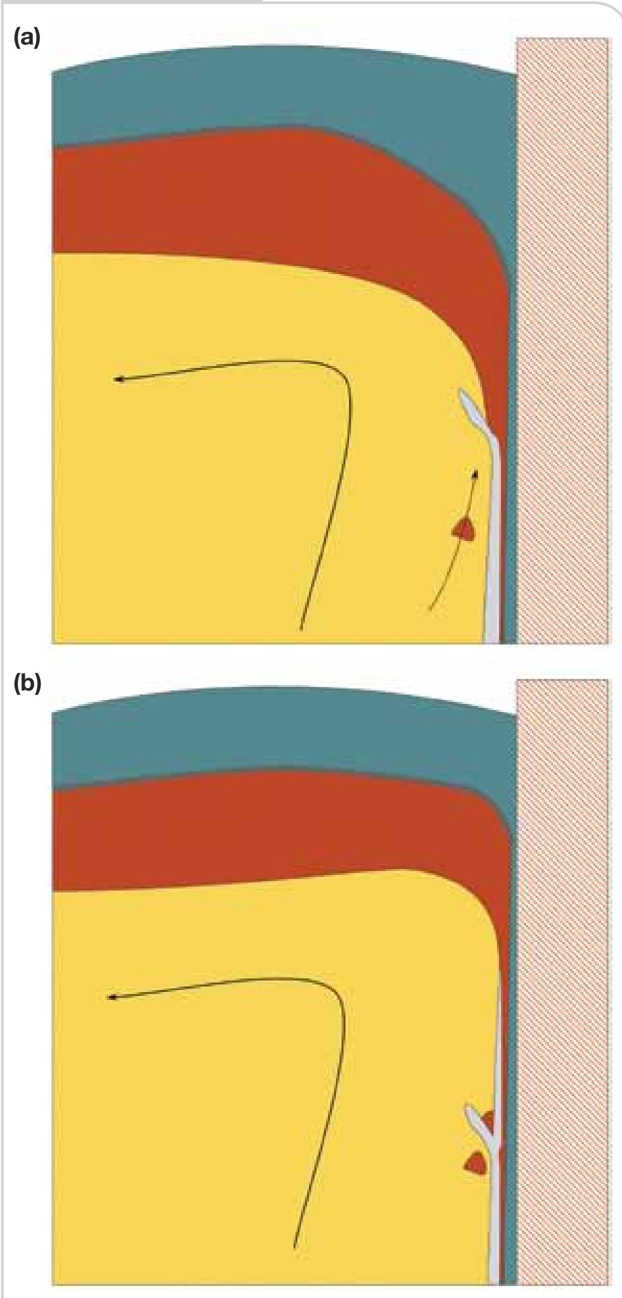

Entrainment by hooks: hook formation and rising particle (a) and slag entrapment on back of hook and particle capture (b).

The jet impinges onto the narrowface with collision speed V_{coll} and angle below horizontal θ_{coll}, and h_{coll} is the depth of the impingement point below the top surface, as illustrated in Figure 2. The collision speed increases with increasing casting speed[15,20] and decreasing slab width.[20] The depth of the impingement point h_{coll} increases with increasing slab width,[20] increasing SEN immersion depth,[20] and decreasing argon gas flowrate.[16]

Plant experiments showed[14,30] good final surface quality is achieved by keeping the "*F* Value" between 3 and 5 N/m[15] (grade not given), or between 2 and 3 N/m[31] for a low-carbon aluminum-killed steel. Considering that the surface velocity $V_{surface}$ in m/second is related to level fluctuation amplitude δ in mm by $V_{surface} = \delta/35$, and that the amplitude of level fluctuations increases linearly with F as approximately $\delta = 3F$,[14,15] these recommendations translate to keeping the surface velocity between 0.26 and 0.43 m/second. The lower limit likely is related to defects caused by meniscus freezing, discussed further in the section entitled, "Meniscus Freezing and Hook Formation," and the upper limit likely is related to interfacial shear phenomena, discussed in the sections "Shear-Layer Instability" and "Upward Flow Impinging Upon the Top Surface."

Meniscus Freezing and Hook Formation

A mechanism for the entrainment of slag and inclusion particles to form surface defects is illustrated in Figure 3, which shows a slag particle being captured by a hook. The root cause of hook formation is freezing of the meniscus[32,33] due to insufficient heat delivered to the meniscus region, particularly near the narrowface, where temperatures tend to be lowest. The frozen meniscus can extend into the melt where it captures rising bubbles, slag droplets or solid inclusions. Additionally, when the molten steel supported above the frozen meniscus overflows, it can carry and entrap slag into the space just above the hook. Hooks can be prevented by increasing superheat, aiming the SEN port angles more upward, or increasing the flow velocity, all of which increase the heat supplied to the meniscus region.

Flow conditions such as those produced by a shallow SEN may produce excessive meniscus velocities, which increase surface turbulence, leading to instability, entrainment, and uneven mold powder distribution, as discussed in the section entitled, "Top Surface Fluctuations." However, too large of an SEN immersion depth can result in shell thinning below mold exit,[20] top surface freezing ("bridging"), and hook formation. Electromagnetic flow control systems have been used[14] to increase flow velocities at lower casting speeds and higher strand widths to avoid hook formation. This meniscus freezing phenomenon imposes a lower limit on surface velocities, perhaps corresponding to that of the flow criteria discussed in section entitled, "Top Surface Fluctuations."

Vortex Formation

Flow past bluff bodies such as an SEN can cause periodic shedding of vortices in the wake of the object, known as a von Kármán vortex street. These vortices can pull slag down into the molten steel, as shown in Figure 4. Any asymmetry between the sides of the mold in the flow pattern, including those caused by turbulent flow, can result in the formation of vortices around the SEN in one of four locations near the SEN,[17,34] although vortex formation does not guarantee slag entrainment. Strong vortices that form and stay near the SEN can entrain slag that becomes entrapped in the solidifying dendrites on the wide face, resulting in increased sliver defects in the center of slabs.[20] As shown in Figure 4c, vortices also may pull a funnel of slag deep enough into the molten steel pool such that the jet leaving the SEN breaks apart the tip of the vortex,[34–37] transporting droplets of slag anywhere in the molten steel pool. Asymmetric flow is reported to increase the frequency, depth and size of the vortices.[38] Asymmetric flow in the mold is caused by SEN clogging,[21,39] asymmetric flow across the bottom of the tundish,[40,41] stopper-rod misalignment,[4,34,42] use of a slidegate mechanism to control throughput,[43,44] turbulent fluctuations,[34,42] and other random asymmetries, such as coalescence of argon bubbles in the SEN sending a large argon bubble out of one port and not the other.[4,19]

Figure 4

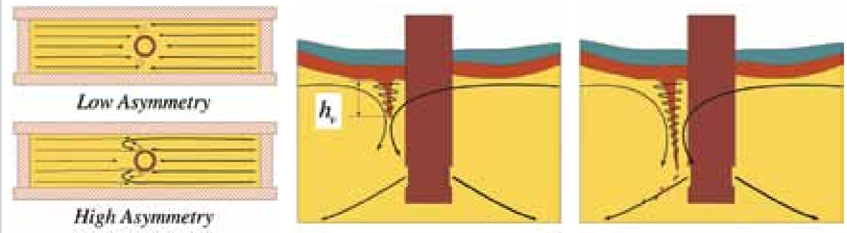

(a) (b) (c)

Entrainment by von Kármán vortex formation: vortexing from asymmetric flow (a); subcritical vortex formation (b); and entrainment by deep vortex (c).

Vortices always are observed to form on the weaker (leeward) side of the flow, i.e., in the wake of the SEN.[17,34–38,45,46] Vortex depth increases with increasing top surface velocity.[36,45] Vortex diameter increases with increasing SEN misalignment in either the width[36] or the thickness[37] directions. Vortex formation frequency increases with increasing SEN flowrate,[20,35,37,45] increasing SEN misalignment,[36,37] aiming the SEN port angles more upward,[35,37] and increasing strand width.[17,20] Vortex formation frequency also increases with more shallow SEN immersion depths,[17,20,35] and there is a critical immersion depth that suppresses vortex formation (100 mm in the water model).[35] Vortex formation can be caused by misaligned stopper rods.[34,42] Vortex formation also is a function of SEN geometry.[17,20] The lifetime/duration of a vortex varies, but it eventually will be damped out by viscous dissipation or changing flow characteristics.[35,45]

Vortex formation needs both rotational flow in the plane of the top surface (from asymmetric flow) and a downward-pulling sink.[38] In double-roll flow patterns, the sink momentum is created where the opposing rolls meet near the center of the mold.[38,45] Vortices were observed on the slower side of the mold moments after a peak in velocity on the opposite side.[45] A sudden jump in downward velocity pulls the vortices deeper into the molten steel pool, enabling the jet to entrain slag from the tip of the funnel.[35] A maximum velocity for vortex formation also was observed, because excessive velocities cause the meniscus to become too oscillatory and turbulent to allow for the formation of vortices.[35,45]

Computational models have reported that vortices cannot occur with perfectly symmetric mold and SEN geometry and symmetric steady-state flow conditions,[36,47] regardless of the mesh size and turbulence model.[47] Realistic flow conditions, however, always produce transient asymmetries. In general, the more misaligned the SEN, the more asymmetric the flow pattern in the mold and the larger the vortex diameter.[36,37] However, the amount of misalignment does not change the downward velocity that helps vortex formation.[36]

Argon flowrates with more than 10% gas fraction induce buoyancy forces that can decrease the downward velocity near the SEN and prevent vortex formation, but that much argon reinforces asymmetric flow[36] and also can trigger some of the argon-related entrainment mechanisms discussed in the section entitled, "Argon Bubble Interactions." Electromagnetic flow control systems can be used to control flow asymmetry and effectively supress vortex formation,[36,46] but the flow control system settings depend on the SEN geometry.[46] Use of both argon gas and electromagnetic flow control systems together can be effective in suppresing vortex formation for a given set of mold and SEN geometry.[36]

Vortex formation frequency f_v (vortices per minute) was observed in water models[15] to increase with increasing F value given by Equation 1, according to $f_v = 3/2F - 10$ at maximum (for $F > 7$) and $f_v = 1/2F$, on average. Another water model study[35] reported no vortex formation below an SEN flowrate of Q_{SEN} = 35 L/minute, and above this limit the formation frequency increased with flowrate at about $Q_{SEN}/20$, where the slope depends on the properties of the slag (oil) layer.

A water model study[48] determined the SEN port velocity at which slag is entrained $V_{port,crit}$ to be:

$$V_{\text{port,crit}} = \sqrt{g w_{\text{strand}} (1-r)(c_1 + c_2 m)} \qquad \text{(Eq. 2)}$$

where

w_{strand} is the strand width, and the constants were fit as $c_1 = 0.1$ and $c_2 = 0.009167$ for 0 mm-deep SEN wells and

$c_1 = 0.35$ and $c_2 = 0.01833$ for 10 mm and deeper SEN wells.

Another water model study[35] proposed a critical surface velocity of 0.3 m/second to form vortices, and the depth of a vortex h_V may be predicted by:

$$h_V = \frac{V_{\text{mc}}^2}{g}\frac{1}{1-r} + c\left(\frac{\Delta V_{\text{s}}^2}{g}\frac{r}{1-r}\right)^{0.55} \qquad \text{(Eq. 3)}$$

where

V_{mc} and ΔV_s are velocites at two specific locations in the melt and

$c = 0.0562\ \text{m}^{0.45}$ is a constant with all other quantities is m-kg-s units. To avoid entrainment by this mechanism, the SEN immersion depth should be greater than the vortex depth.[35]

The amount of slag entrained by vortices was measured experimentally[49,50] for molten steel and several slags. This prediction of entrained mass can be used to predict particle diameter as:

$$d = \sqrt[3]{\frac{6}{\pi}\frac{1}{\rho_{\text{u}}}\left(\frac{c}{\mu_{\text{u}}^{0.255}\Gamma_{\text{u}\ell}^{2.18}}\right)} \qquad \text{(Eq. 4)}$$

where

$c = 3.057\ \text{kg}^{3.435}\cdot\text{m}^{-0.255}\cdot\text{s}^{-4.615}$ is a constant,
is the slag viscosity in Pa·s, and

$\Gamma_{u\ell}$ is the interfacial tension in N/m, to give the mass (the term in parentheses) in kg. Slags with higher viscosity and higher interfacial tension yield smaller amounts of entrained slag.

Shear-Layer Instability

The interface between two density-stratified fluids with relative motion will become unstable with a sufficiently large difference in velocity. Most studies of slag entrainment have identified this phenomenon, known as Kelvin–Helmholtz instability (KHI), as a cause of mold slag entrainment, as shown in Figure 5. This shear instability mechanism is most likely to occur halfway between the narrowface and the SEN, where the horizontal surface velocity is largest.

A theoretical condition for this instability was first explored by Helmholtz,[51] but predicted instability at all velocity differences; Kelvin[52] added surface tension to get a model that provides a critical velocity difference of:

$$\Delta V_{\text{crit}} = \sqrt[4]{4g\left(\rho_\ell - \rho_{\text{u}}\right)\Gamma_{\text{u}\ell}\left(\frac{1}{\rho_{\text{u}}} + \frac{1}{\rho_\ell}\right)^2} \qquad \text{(Eq. 5)}$$

An alternative prediction[53] of the Kelvin–Helmholtz instability for finite layer thickness, inviscid fluids and zero interfacial tension gives a critical velocity of:

Figure 5

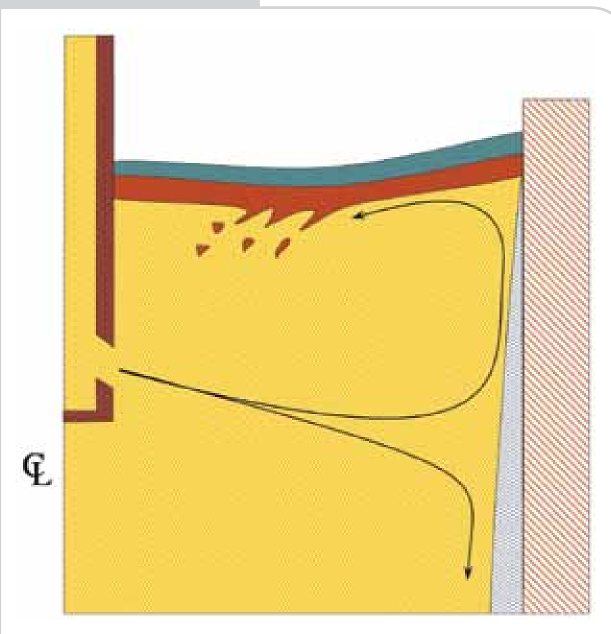

Shear-layer instability.

Figure 6

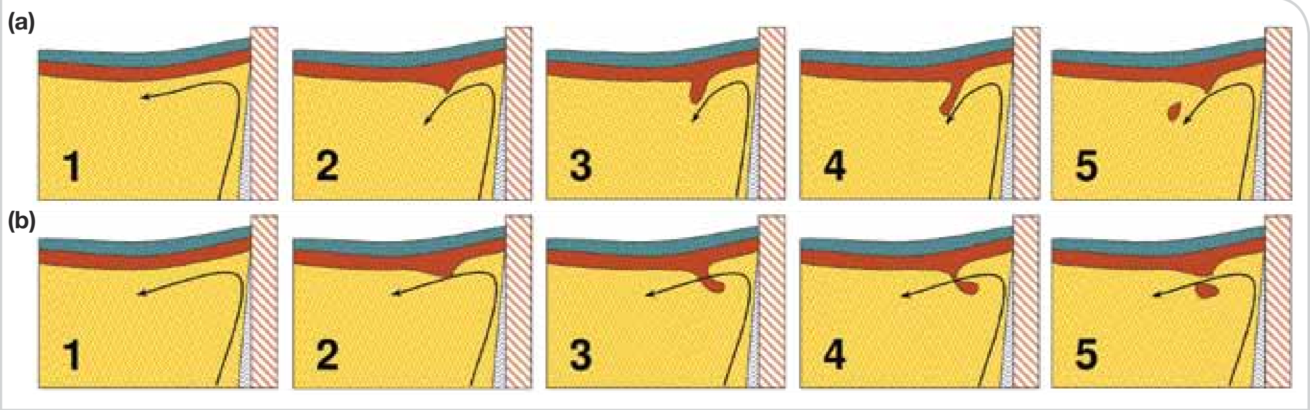

Entrainment by impinging flow upon the top surface: time sequence of entrainment by dragging mode (a), and time sequence of entrainment by cutting mode (b).

$$\Delta V_{\mathrm{crit}} = \sqrt{g(\rho_\ell - \rho_{\mathrm{u}})\left(\frac{h_{\mathrm{u}}}{\rho_{\mathrm{u}}} + \frac{h_\ell}{\rho_\ell}\right)} \quad \text{(Eq. 6)}$$

where

h_u and h_ℓ are the thicknesses of the upper and lower layers.

The validity of Equation 6 was confirmed in experiments[54] of a rotating covered trough for low-viscosity oils and low-frequency perturbations where interfacial tension is not dominant. The Kelvin–Helmholtz theory was generalized[55] to include the effects of viscosity as"

$$\Delta V_{\mathrm{crit}} = \sqrt[4]{4g(\rho_\ell - \rho_{\mathrm{u}})\Gamma_{\mathrm{u}\ell}\frac{(\mu_\ell + \mu_{\mathrm{u}})^4}{(\rho_{\mathrm{u}}\mu_\ell^2 + \rho_\ell\mu_{\mathrm{u}}^2)^2}} \quad \text{(Eq. 7)}$$

The viscous solution produces a lower critical velocity than the inviscid solution; this counter-intuitive result is due to the additional momentum transfer caused by shear stresses. Equation 7 reduces to Equation 5 when the kinematic shear viscosities (μ/ρ) are equal in the two fluids, or when the density ratio equals the viscosity ratio.[55]

The stability of the interface is not affected by a magnetic field directed transverse to the flow,[56,57] i.e., DC electromagnetic flow control. A magnetic field applied parallel to the flow direction stabilizes the interface analogous to interfacial tension.[56] Numerical studies of a continuous caster[57] that included interfacial tension and induced current effects from the finite-conducting steel shell showed that the parallel magnetic field adds to the effect of interfacial tension and damps out the instability flow structures, but does not affect the critical interface velocity.

Upward Flow Impinging Upon the Top Surface

The upward spout along the narrowfaces resulting from a double-roll flow pattern may cause slag entrainment in either a dragging[58] or cutting[59] fashion, as illustrated in Figures 6a and 6b. This is an example of shear-layer instability where the additional geometric aspects of the flow render the Kelvin-Helmholtz theory inapplicable.

The first model of slag entrainment[60] proposed that entrainment occurs when the kinetic energy of a circular slag particle with diameter d exceeds the energy cost to form the particle surface and work done by the buoyancy force through a distance of one-half the particle diameter, giving a cricital surface velocity of:

$$V_{\mathrm{crit}} = \sqrt[4]{48}\sqrt[4]{\frac{g\Gamma_{\mathrm{u}\ell}}{\rho_\ell}}\sqrt[4]{\frac{1}{r^2} - \frac{1}{r}} \quad \text{(Eq. 8)}$$

and accompanying particle diameter of:

$$d = \sqrt{12}\sqrt{\frac{\Gamma_{\mathrm{u}\ell}}{g(\rho_\ell - \rho_{\mathrm{u}})}} \quad \text{(Eq. 9)}$$

An extension[61] of this first work includes the work done by the weight of the slag particle during a top surface level fluctuation with amplitude δ, giving a critical velocity of:

$$V_{\text{crit}} = \sqrt{\sqrt{48}\sqrt{\frac{g\Gamma_{\text{u}\ell}}{\rho_\ell}}\sqrt{\frac{1}{r^2}-\frac{3}{r}}-2g\delta}$$

(Eq. 10)

which is limited to slags with density less than one-third that of steel. Another proposed criterion for entrainment[16] is that the radius of curvature of the interface is smaller than produced droplet radius, giving the critical interface velocity of:

$$V_{\text{crit}} = \sqrt{\sqrt{8}\sqrt[4]{\frac{g\Gamma_{\text{u}\ell}}{\rho_\ell}}\sqrt[4]{1-r}}$$

(Eq. 11)

and droplet diameter of:

$$d = 2\sqrt{\frac{\Gamma_{\text{u}\ell}}{g\left(\rho_\ell-\rho_{\text{u}}\right)}}$$

(Eq. 12)

An oil-and-water physical model study[62] used a submerged rotating cylinder to duplicate the flow field caused by the narrowface spout. The proposed criterion for entrainment is a critical capillary number as a function of the ratio of kinematic shear viscosities:

$$V_{\text{crit}} = \frac{\Gamma_{\text{u}\ell}}{\mu_\ell}\left(c_1 + c_2\frac{\mu_{\text{u}}/\rho_{\text{u}}}{\mu_\ell/\rho_\ell}\right)$$

(Eq. 13)

where

$c_1 = 2.8 \times 10^{-3}$ and $c_2 = 3 \times 10^{-6}$ are fitting constants.

An oil-and-water physical model study[59] reported a critical surface velocity of 0.116 m/second for this mechanism, which motivated a later study[58] that proposed the relation:

$$V_{\text{crit}} = 3.065\frac{\Gamma_{\text{u}\ell}^{0.292}g^{0.115}}{h_{\text{u}}^{0.356}}\frac{\left(\rho_\ell-\rho_{\text{u}}\right)^{0.215}}{\rho_{\text{u}}^{0.694}}\frac{\mu_{\text{u}}^{0.231}}{\mu_\ell^{0.043}}$$

(Eq. 14)

for the critical velocity. Equation 14 was fit to measurements of an oil-and-water apparatus that used a submerged hose aimed at a wall to create the upward impinging flow pattern. The exponents in this model appear to be reasonable given the theoretical developments discussed in this section. The quantitative predictions of this model are reasonable for a steel-slag system, and the qualitative behavior is clear: entrainment occurs more easily with smaller interfacial tension, smaller slag viscosity and larger liquid slag layer thickness, h_{u}. The measured critical velocities were sensitive to the interfacial tension, but the density and surface tension were changed together using additives.[58] Several droplets were entrained by the shearing flow, and the first entrained droplet always was the largest, with the diameter given by:

$$d = 0.534\frac{\Gamma_{\text{u}\ell}^{0.693}}{g^{0.564}\left(\rho_\ell-\rho_{\text{u}}\right)^{0.130}\rho_{\text{u}}^{0.306}}\frac{\mu_{\text{u}}^{0.114}}{\mu_\ell^{0.372}}$$

(Eq. 15)

This study was repeated[63] with a wider range of properties, more controlled flow patterns and reported similar trends except for the effect of slag layer thickness; the difference might be due to variations in the angle of attack of the water jet. The important parameters for entrainment by this mechanism are, in order: interfacial tension, mass density difference, dynamic shear viscosity and slag layer thickness.

A similar entrainment mechanism occurs in ladle metallurgy. Combined oil-and-water experiments[64,65] and multiphase numerical models[66] of a system that creates flow patterns similar to those found in continuous casting showed that shear-layer (Kelvin–Helmholtz) instability is the dominant mechanism for entraining slag in ladles, with a critical surface velocity of about 0.26 m/second. An oil-and-water physical model study[67] of a ladle found that entrainment occurs at a critical velocity of 0.233 m/second, which motivated the entrainment criterion of a critical density-modified Weber number of 12.3, giving critical velocity prediction of:

$$V_{\text{crit}} = \sqrt{12.3}\sqrt[4]{\frac{g\Gamma_{\text{u}\ell}}{\rho_\ell}}\sqrt[4]{1-r}$$

(Eq. 16)

Some researchers[63] have suggested that such simple Weber-number relationships cannot make accurate predictions in systems as complicated as a continuous casting mold. This statement likely is true and the original researchers made a serendipitous choice with the Weber number. This critical value of 12.3 for the Weber number $\mathrm{We}_{\mathrm{crit}} = \rho_u V_{\mathrm{crit}}^2 L / \Gamma_{u\ell}$ may be explained by assuming that the shear-layer instability mechanism causes the entrainment. Taking the critical velocity from the Kelvin–Helmholtz theory (Equation 5) and one-half of the capillary wavelength, $2\pi\sqrt{\Gamma_{u\ell} / g(\rho_\ell - \rho_u)}$, as the characteristic velocity and length, the critical Weber number is $\mathrm{We}_{\mathrm{crit}} = 2\pi(1+r)$; using a density ratio of 0.98, typical for oil and water (property values not given in the original reference), this expression evaluates to 12.4. For density ratios appropriate for slag-and-steel systems this critical Weber number is about 8 to 9.

A theoretical model of the balance between inertia, interfacial tension, and buoyancy at the slag-steel interface in a ladle gives the critical surface velocity[68] as:

$$V_{\mathrm{crit}} = \sqrt[4]{\frac{128}{3}\cos(\alpha)}\sqrt[4]{\frac{g\Gamma_{u\ell}}{\rho_\ell}}\sqrt[4]{\frac{1}{r^2} - \frac{1}{r}} \tag{Eq. 17}$$

where α is the angle between the interface and the direction of gravity. The diameter of the corresponding droplet size is:

$$d = \sqrt{\frac{6}{\cos(\alpha)}}\sqrt{\frac{\Gamma_{u\ell}}{g(\rho_\ell - \rho_u)}} \tag{Eq. 18}$$

This model should be applied with care for nearly horizontal interfaces.

Argon Bubble Interactions

The interaction of the molten steel and slag flows with argon gas bubbles leads to another family of entrainment mechanisms. Argon gas usually is fed into the SEN to help prevent SEN clogging, which causes problems with nonmetallic inclusions and asymmetric fluid flow.[21] Argon bubbles also add a buoyancy force to the steel flow that lifts the jet upwards toward the steel/slag interface,[16,23,69] changing the flow pattern. Argon gas can alleviate some problems, such as meniscus freezing and vortex formation, but can aggravate other entrainment mechanisms, such as the top surface fluctuations. Additionally, nonmetallic inclusions and slag can adhere to the surface of argon bubbles,[59] leading to large defects if entrapped in the final product.

A water model study[59] showed that gas bubbles flowing out of the SEN can form a foam with the oil (slag) layer, illustrated in Figure 7a. This foam then can adhere to and crawl down the outside of the SEN and break apart in the jet, which entrains large amounts of slag, as shown in Figure 7b. The formation of this slag foam leads to entrainment defects despite small mold surface velocity and level fluctuations.[59]

The occurrence of the foam increases with decreasing bubble diameters, increasing strand width, increasing argon gas flowrate, increasing slag viscosity, decreasing slag mass density, and decreasing interfacial tension between the slag and steel.[59] Other water model experiments[19] observed that this critical argon flow rate decreases with increasing SEN flowrate, decreasing slag viscosity, aiming the SEN port angles more upward, and decreasing wettability between the SEN material and molten slag. Some plant trials[59] showed a reduction of pencil-pipe defects with reduced argon flowrate, but other plant trials[70] showed that the number of pencil blister defects correlates strongly with overall throughput and is insensitive to argon flowrate, SEN port angles, SEN port diameter and SEN submergence depth.

As a bubble rises into and through the molten slag layer, a thin film of molten steel is caught between the bubble and the slag. If the bubble breaks through to the atmosphere, the film of steel will be trapped in the slag layer until gravity pulls it back into the melt, possibly bringing some slag with it,[71,72] as shown in Figure 8. Physical model investigations revealed that the maximum

Figure 7

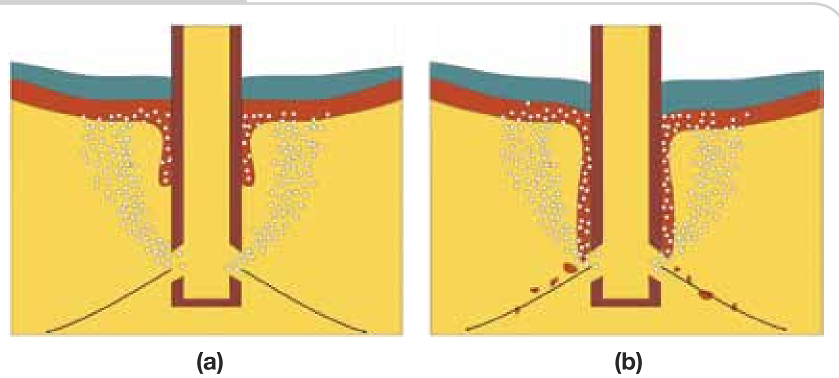

Slag foaming: foam formation (a); and entrainment due to slag foam (b).

Figure 8

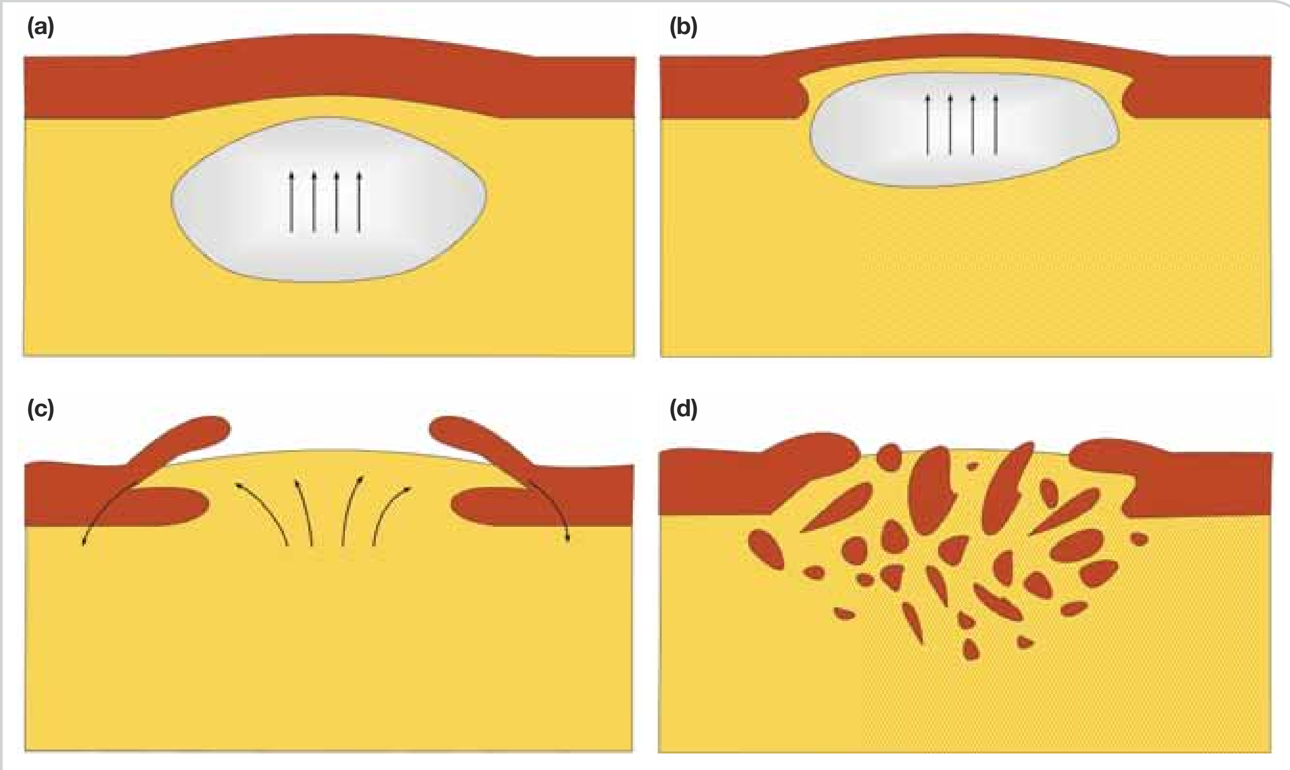

Entrainment by bubble penetration of slag layer: approaching bubble (a); penetrating bubble (b); slag layer rupture (c); and entrainment after rupture (d).

depth the slag is carried downward into the molten steel after bubble penetration into the slag layer was consistently about three times the bubble diameter.[72] Smaller bubbles were observed to not rupture the slag layer at all.[71] The physical properties of the fluids had almost no effect on this phenomenon, except that increasing the interfacial tension likely decreases the slag entrainment.[72] However, the flow inside the liquid slag layer[73,74] and the constraint provided by the sintered slag layer,[72] forces the bubbles to move laterally toward the SEN or narrowface, somewhat mitigating the entrainment by this mechanism.

Slag Crawling

A solid object submerged into a flowing liquid causes a pressure buildup on the windward (right) side and a corresponding pressure drop in the leeward (left) side, as illustrated in Figure 9a. In the presence of a free surface this pressure difference changes the position of the surface. Asymmetric flow in a continuous casting mold can cause this situation to occur with the SEN. The low-pressure zone can draw liquid slag down along the leeward exterior surface of the SEN, as shown in Figure 9a. If this effect is severe enough, and the SEN depth is shallow enough, then the slag can crawl down the SEN walls and be carried away into the molten steel pool by the steel jet, as shown in Figure 9b.

Physical model experiments of flow past a circular cylinder in a rotating trough[75] investigated the effect of fluid properties on this entrainment mechanism. For casters with the ratio of SEN outer diameter to slab thickness, or "blockage factor," between 0.4 and 0.6, the penetration depth h_p that the upper fluid crawls down the cylinder is:

$$h_p = 1.9\frac{c_{p,\max}\rho_u V_u^2 + c_{p,\min}\rho_\ell V_\ell^2}{g\left(\rho_\ell - \rho_u\right)} \quad \text{(Eq. 19)}$$

where

$C_{p,\max} = 1.0$ and $C_{p,\min} = 2.5$ are the maximum and minimum pressure coefficients for a circular SEN.

The maximum pressure coefficient occurs at the forward stagnation point (windward side) and the minimum pressure coefficient occurs on the sides of the SEN, closest to the wide faces. For elliptical SENs,

Figure 9

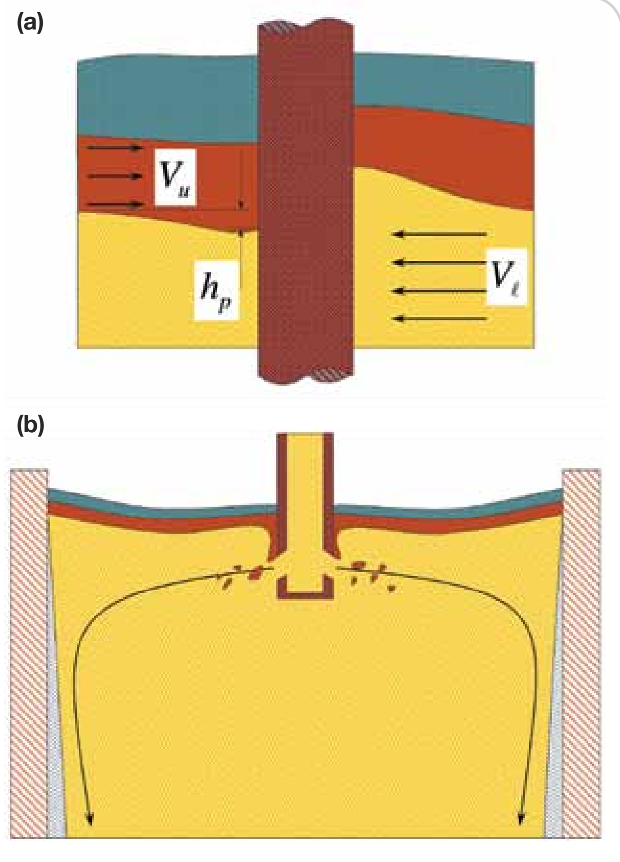

Slag crawling model (a) and entrainment by slag crawling (b).

a numerical study found that these pressure coefficients decrease with increasing aspect ratio;[76] increasing the SEN aspect ratio reduces the slag penetration depth by reducing the pressure drop across the SEN. Slag entrainment by this mechanism is avoided with the SEN immersion depth greater than the slag penetration depth.[75]

The flow in these experiments was in the same direction on both sides of the SEN; in a caster, the two flows oppose each other near the SEN, so Equation 19 may be an overprediction of penetration depth in practice. However, the downward component of the molten steel flow near the SEN in double-roll flow can help the slag to crawl down the SEN. Additionally, the negative pressure zone often found in the top of SEN ports might assist the crawling action, though the negative pressure in the ports is not strong enough to cause entrainment by itself[20,21] for reasonable immersion depths. Water model studies[59] observed a critical minimum immersion depth that causes immediate entrainment of a large number of small slag droplets, due to the combination of slag crawling, downward flow and negative pressure at the top of the SEN ports. Slag crawling and the slag foaming mechanism discussed in the previous section can act together to cause entrainment,[59] but this effect is not reflected in Equation 19.

Water model studies[19,71] observed that the oil layer was drawn downward via capillary action along the gas-filled spaces of the rough surface of the SEN, which was coated with a wax to decrease wettability. This capillary action may also be an entrainment mechanism in continuous casting molds.

Top Surface Standing Wave Instability

Flow beneath a free liquid surface will create surface waves that become unstable if the local slope becomes too steep,[77] i.e., exceeding vertical, entraining one fluid into the other. This phenomenon is relevant at the top surface of the molten steel pool in continuous casting, where flow in the mold produces a standing wave at the surface. The standing wave also may become unstable if the vertical acceleration of the fluid is greater than the gravitational acceleration,[78,79] although this appears not to be a problem in practice.[25] This standing wave has a wavelength on the order of half of the mold width, in contrast to the smaller fluctuations discussed in earlier. The top surface usually is raised near the narrow faces for double-roll flow patterns; however, sufficient argon flowrates can raise the top surface near the SEN.[19]

A numerical investigation[77] explored the stability of two-dimensional standing waves at the interface between two inviscid, irrotational and incompressible fluids of different but uniform density in an infinite domain. The results of this study were reduced[80] to the height-to-wavelength stability criterion of:

$$\left(\frac{h_{\mathrm{wave}}}{\lambda}\right)_{\mathrm{crit}} = 0.21 + 0.14r^2$$

(Eq. 20)

where

h_{wave} is the wave height, defined for a caster as the vertical distance between the lowest point (trough) and highest point (crest) of the surface level, and

λ is the wavelength, defined for a caster as the distance between the outer SEN wall and the narrowfaces,[25,80,81] although the value of λ does increase as SEN immersion depth h_{SEN} decreases.[81]

As the density ratio ρ_u/ρ_ℓ decreases, the higher harmonics of the wave are damped out and the location of vertical slope shifts from the midpoint of the wave toward the crest.[77] Physical[82] and numerical[83] experiments show that a vortex forms at the wave node at lower height-to-wavelength ratios predicted by Equation 20, indicating that the stability of the wave is governed by shearing at the interface between the fluids, rather than the wave turning over.[77]

Although derived for conditions different from a continuous caster, Equation 20 has been used to classify the critical wave height. The models in the literature[17,22,25,80,84] report that the height of the standing wave behaves like:

$$h_{\mathrm{wave}} = c\frac{V_{\mathrm{port}}^2}{g}\frac{d_{\mathrm{port}}}{L_{\mathrm{URZ}}}f(r)$$

(Eq. 21)

where

c is a numerical constant,
$f(r)$ is a function of the density ratio,
d_{port} is the diameter of the SEN ports, V_{port} is the velocity of the water or molten steel at the SEN ports, and
L_{URZ} is a characteristic length of the upper recirculation zone, calculated from the geometry shown in Figure 10 as

$$L_{\mathrm{URZ}} = h_{\mathrm{SEN}} + \frac{1}{2}w_{\mathrm{strand}}\tan\left(\theta_{\mathrm{d}} - \frac{1}{2}\theta_{\mathrm{j}}\right)$$

(Eq. 22)

where

h_{SEN} is the SEN immersion depth,
w_{strand} is the strand width,
θ_{d} is the jet discharge angle, and
θ_{j} is the jet spread angle.

The jet discharge angle is independent of flowrate,[85] is independent of port width,[85] aims more upward with increasing argon flowrate,[44] aims more downward with more downward lower port angle,[44,85,86] and is always more downward than the port angle.[85,86] The jet discharge angle becomes closer to the lower port angle as the port height decreases and as the SEN wall thickness increases.[85] The jet discharge angle also is a function of the port shape.[44,85] The jet spread angle is independent of flowrate,[85,86] independent of port width,[85] and increases with more upward jet discharge angle.[86] The jet impingement point moves downward with increasing casting speed.[20]

The behavior of the top surface of the molten steel pool is a function of the flow pattern, which depends on throughput, SEN geometry and depth, and electromagnetic flow control systems. Using models based on the Froude number as in Equation 21 may help determine the functional relationship between quantities, but the numerical coefficients have limited applicability outside of the conditions for which they were derived.

The models presented by Equation 21 show that the wave height, h_{wave}, increases with the dynamic head of the flow out of the SEN ports, V_{port}^2/g, because higher casting speeds or throughputs generally increase all velocities in the molten steel pool. Some researchers report[26] a linear relationship between wave height and casting speed, in contrast with the quadratic relationship given in the models presented in this section, while others report something in between.[81,87] The wave height increases with increasing density ratio,[80,84] decreasing SEN immersion depth,[17,81,84,87] aiming the SEN port angles more upward,[17,26,84,87] narrower strand widths[1,17] and narrower strand thicknesses.[1] One study[17] reports that the wave height increases with increasing SEN port diameter, while another[87] claims the reverse.

The initial numerical investigations[25,80,81] into this entrainment mechanism assumed isothermal, room-temperature fluid flow and were not able to simulate the wave instability. Improvements to their interfacial tension calculations in a later 2D air-and-water simulation[83] of a water model[17] successfully simulated the wave turning over and the resulting entrainment of air bubbles at the trough of the wave. A 3D single-phase numerical model of a thin-slab caster[87] that included the effect of temperature gradients and buoyancy showed a large increase in wave height because of the thermal effects. Other studies in thin-slab casters[1,88]

Figure 10

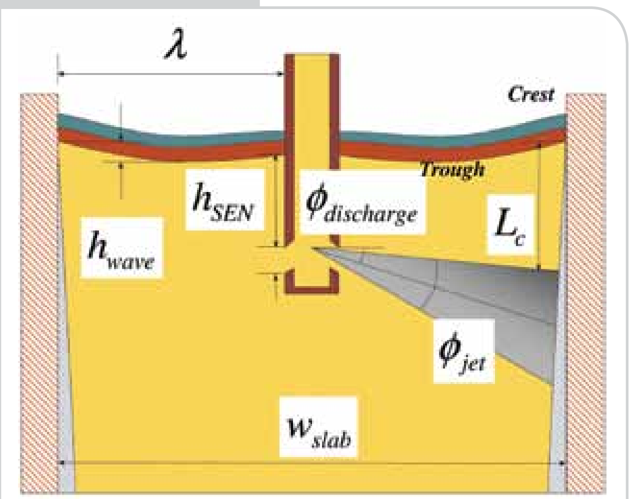

Top surface standing wave model description.

show that the presence of the shell (in the smaller liquid pool relative to thick-slab casters) affects all aspects of the flow pattern, including the top surface velocities and wave height.

The numerical study[83] with improved interfacial tension calculations showed a recirculating packet of fluid at the wave trough that disappeared after the instability event, which suggests that a vortex (with axis running between the wide faces) contributes to the instability of the interface. The highest surface velocities are found at the trough of the standing wave,[48,81,83] which further supports the idea that the stability of the top surface is governed by the shearing stresses at the interface, discussed earlier, and not the wave-turnover mechanism (as was indicated in the original reference[77]). However, none of the studies mentioned in this section investigated a real steel-slag system, and none of the computational models included all of the relevant physical phenomena in the same model.

Top Surface Balding

Some of the flow phenomena discussed above can be taken to the extreme of pushing the slag layer to the sides of the top surface, as illustrated in Figure 11a for excessive impinging flow upon the top surface.[48] This phenomenon was termed "balding" of the surface, as it exposes molten steel to the atmosphere, if not the sintered and solid powder layers of the slag layer. This well-known phenomenon in ladle refining, there known as an "eye," also can occur in continuous casting molds at high SEN flowrates, and the accompanying surface reoxidation forms inclusions such as alumina. Particles of mold powder can become entrained at the bald meniscus, especially if the bald spot coincides with the trough of the standing wave.[48] Meniscus balding is prevented by having a minimum slag layer thickness of at least the size of the standing wave height,[84] such as predicted from one of Equation 21. Meniscus balding also can be caused by high argon flowrates,[18] as illustrated in Figure 11b.

Figure 11

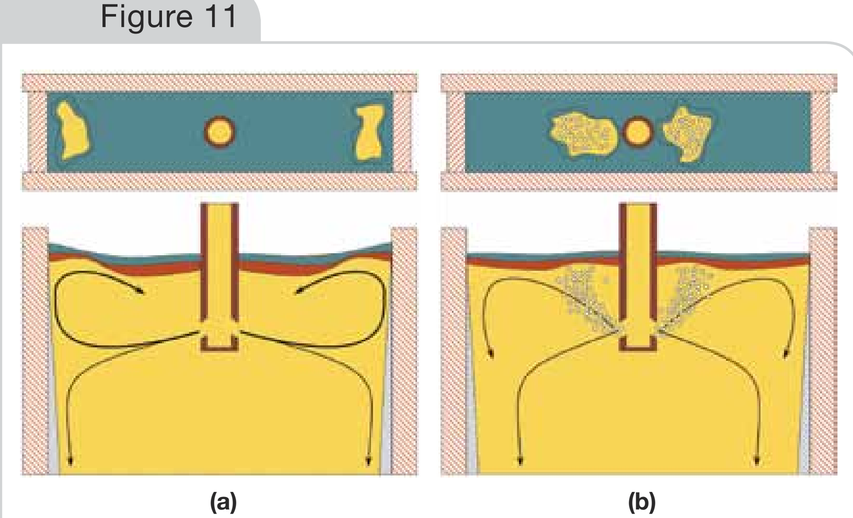

Balding by excessive nf spout.

Determining the Safe Operating Window

Designing a caster to avoid mold slag entrainment requires the careful selection of many different parameters to find the window of stable, entrainment-free operation. The casting conditions must be chosen to avoid simultaneously each of the above mechanisms.

Like in most engineering problems, the prevention of entrainment involves many trade-offs. For example, the choice of slag layer properties must balance the conflicting needs to use the slag to capture inclusions, which requires lower interfacial tension, and to prevent shear-layer instability, which requires higher interfacial tension. Preventing entrainment by both top surface fluctuations and shear-layer instability requires control of the top surface velocities with proper selection of SEN parameters and electromagnetic flow control settings. However, the meniscus temperatures must remain high enough to prevent the formation of hooks.

The models presented in this article can be used together as design tools or to evaluate the results of physical or numerical models of flow in a caster. Note that the different mechanisms can act together, which affects the entrainment criteria. For example, the critical velocity condition for a given mechanism can be exceeded with asymmetric flow (which also creates entrainment by vortex formation), even though the symmetric time-averaged flow conditions yield no risk of entrainment. Uneven SEN clogging often is responsible for such asymmetric flow patterns, with top surface velocities easily doubling their unclogged values;[21] see also the discussion of asymmetric flow in the "Slag Crawling" section.

Conclusions

Many studies have been performed over the years to investigate mold slag entrainment, which is one of the main sources of inclusion defects in the continuous casting of steel. This review article identified nine distinct mechanisms responsible for mold slag entrainment: top surface-level fluctuations, meniscus freezing, vortexing, shear-layer instability, narrowface spout impingement upon the top surface, and argon bubble interactions. The slag layer can also crawl down the SEN, but this effect is an issue only at very shallow submergence depths, or when combined with the slag foaming with argon bubbles. Another mechanism, the instability of the top surface standing wave, appears unimportant because shear-layer instability occurs more easily. Extreme flow conditions result in the "balding" of the top surface and should be avoided. The various simple models available to estimate these nine mechanisms are summarized in this article, which can be used together to evaluate the quality of flow patterns found from physical or numerical models of flow in the continuous casting process.

Acknowledgments

The authors gratefully acknowledge the financial support of the member companies of the Continuous Casting Consortium at the University of Illinois at Urbana-Champaign. The authors thank Junya Iwasaki of Nippon Steel Co. for translation of some of the references.

References

1. R. Chaudhary, B.T. Rietow and B.G. Thomas, "Differences Between Physical Water Models and Steel Continuous Casters: A Theoretical Evaluation," *Proceedings of the Materials Science and Technology Conference,* pp. 1090–1101, ACerS/AIST/ASM/TMS, 2009.
2. Q. Yuan and B.G. Thomas, "Transport and Entrapment of Particles in Continuous Casting of Steel," *Proceedings of 3 International Congress on Science and Technology of Steelmaking,* pp. 745–762, Association for Iron & Steel Technology, 2005.
3. Q. Yuan and B.G. Thomas, "Transport and Entrapment of Particles in Continuous Casting of Steel," *Proceedings of Modeling of Casting, Welding, and Advanced Solidification Processes XI,* pp. 745–752, The Minerals, Metals and Materials Society, 2006.
4. G-G. Lee, H-J. Shin, B.G. Thomas and S-H. Kim, "Asymmetric Multi-Phase Fluid Flow and Particle Entrapment in a Continuous Casting Mold," *AISTech Conference Proceedings,* Vol. II, pp. 63–73, 2008.
5. S. Kunstreich and P.H. Dauby, "Effect of Liquid Steel Flow Pattern on Slab Quality and the Need for Dynamic Electromagnetic Control in the Mold," *Ironmaking and Steelmaking,* Vol. 32, No. 1, pp. 80–86, 2005.
6. A.W. Cramb and I. Jimbo, "Interfacial Considerations in Continuous Casting," *ISS Transactions,* Vol. 11, pp. 67–79, 1990.
7. A.W. Cramb, Y. Chung, J. Harman, A. Sharan and I. Jimbo, "The Slag/Metal Interface and Associated Phenomena," *Iron and Steelmaker,* Vol. 24, No. 3, pp. 77–83, 1997.
8. D. Bouris and G. Bergeles, "Investigation of Inclusion Re-Entrainment From the Steel-Slag Interface," *Metallurgical and Materials Transactions B,* Vol. 29, No. 3, pp. 641–649, 1998.
9. J. Strandh, K. Nakajima, R. Eriksson and P. Jönsson, "A Mathematical Model to Study Liquid Inclusion Behavior at the Steel-Slag Interface," *ISIJ International,* Vol. 45, No. 12, pp. 1838–1847, 2005.
10. C. Ojeda, B.G. Thomas, J. Barco and J. Arana, "Model of Thermal-Fluid Flow in the Meniscus Region During an Oscillation Cycle," *AISTech Conference Proceedings,* Vol. II, pp. 269–283, 2007.
11. J. Sengupta, C. Ojeda and B.G. Thomas, "Thermal-Mechanical Behavior During Initial Solidification in Continuous Casting: Steel Grade Effects," *International Journal of Cast Metals Research,* Vol. 22, No. 1–4, pp. 8–14, 2009.
12. R. Liu, B.G. Thomas, L. Kalra, T. Bhattacharya and A. Dasgupta, "Slidegate Dither Effects on Transient Flow and Mold Level Fluctuations," *AISTech Conference Proceedings,* Vol. II, pp. 1351–1364, 2013.
13. M. Javurek, M. Thumfart, K. Rieger and M. Hirschmanner, "Mathematical Mold Level Model Based on Numerical Simulations and Water Model Experiments," *Proceedings of the 6th European Conference on Continuous Casting,* 2008.
14. J. Kubota, K. Okimoto, A. Shirayama and H. Murakami, "Meniscus Flow Control in the Mold by Traveling Magnetic Field for High-Speed Slab Caster," *74 Steelmaking Conference Proceedings,* pp. 233–241, The Iron and Steel Society, 1991.
15. T. Teshima, M. Osame, K. Okimoto and Y. Nimura, "Improvement of Surface Property of Steel at High Casting Speed," *71 Steelmaking Conference Proceedings,* pp. 111–118, The Iron and Steel Society, 1988.
16. H. Nakato, K. Saito, Y. Oguchi, N. Namura and K. Sorimachi, "Surface Quality Improvement of Continuously Cast Blooms by Optimizing Solidification in Early Stage," *70 Steelmaking Conference Proceedings,* pp. 427–431, The Iron and Steel Society, 1987.
17. D. Gupta and A.K. Lahiri, "Water-Modeling Study of the Surface Disturbances in Continuous Slab Caster," *Metallurgical and Materials Transactions B,* Vol. 25, No. 2, pp. 227–233, 1994.
18. D.J. Harris and J.D. Young, "Water Modeling – A Viable Production Tool," *65 Steelmaking Conference Proceedings,* pp. 3–16, The Iron and Steel Society, 1982.
19. Z. Wang, K. Mukai, Z. Ma, M. Nishi, H. Tsukamoto and F. Shi, "Influence of Injected Ar Gas on the Involvement of the Mold Powder Under Different Wettabilities Between Porous Refractory and Molten Steel," *ISIJ International,* Vol. 39, No. 8, pp. 795–803, 1999.
20. Y.H. Wang, "A Study of the Effect of Casting Conditions on Fluid Flow in the Mold Using Water Modeling," *73 Steelmaking Conference Proceedings,* pp. 473–480, The Iron and Steel Society, 1990.
21. Q. He, G. Evans, R. Serje and T. Jaques, "Fluid Flow and Mold Slag Entrainment in the Continuous Twin-Slab Casting Mold," *AISTech Conference Proceedings,* Vol. 2, pp. 573–588, 2009.
22. B.S. Moghaddam, E. Steinmetz and P.R. Scheller, "Interaction Between the Flow Condition and the Meniscus Disturbance in the Continuous Slab Caster," *Proceedings of the International Congress on the Science and Technology of Steelmaking,* Vol. 3, pp. 911–920, Association for Iron & Steel Technology, 2005.
23. P. Andrzejewski, K-U. Köhler and W. Pluschkell, "Model Investigations on the Fluid Flow in Continuous Casting Molds of Wide Dimensions," *Steel Research,* Vol. 63, No. 6, pp. 242–246, 1992.
24. A. Matsushita, K. Isogami, M. Temma, T. Ninomiya and K. Tsutsumi, "Direct Observation of Molten Steel Meniscus

in CC Mold During Casting," *Transactions of the ISIJ,* Vol. 28, No. 7, pp. 531–534, 1988.

25. G.A. Panaras, A. Theodorakakos and G. Bergeles, "Numerical Investigation of the Free Surface in a Continuous Steel Casting Mold," *Metallurgical and Materials Transactions B,* Vol. 29, No. 5, pp. 1117–1126, 1998.
26. T. Honeyands and J. Herbertson, "Flow Dynamics in Thin Slab Caster Molds," *Steel Research,* Vol. 66, No. 7, pp. 287–293, 1995.
27. R. Chaudhary, B.G. Thomas and S.P. Vanka, "Effect of Electromagnetic Ruler Braking (EMBr) on Transient Turbulent Flow in Continuous Slab Casting Using Large Eddy Simulations," *Metallurgical and Materials Transactions B,* Vol. 43, No. 3, pp. 532–553, 2012.
28. S. Kunstreich, P.H. Dauby, S-K. Baek and S-M. Lee, "Multi-Mode EMS in Thick Slab Caster Molds and Effect on Coil Quality and Machine Performance," *Proceedings of the 5th European Conference on Continuous Casting,* 2005.
29. K. Cukierski and B.G. Thomas, "Flow Control With Local Electromagnetic Braking in Continuous Casting of Steel," *Metallurgical and Materials Transactions B,* Vol. 39, No. 1, pp. 94–107, 2008.
30. J. Kubota, K. Okimoto, M. Suzuki, A. Shirayama and T. Masaoka, "Mechanism of Level Fluctuation and Mold Powder Catching in Slab Continuous Casting at High Speeds," *Proceedings of the 6 International Iron and Steel Congress,* Vol. 3, pp. 356–363, The Iron and Steel Institute of Japan, 1990.
31. H. Nakamura, S. Kohira, J. Kubota, T. Kondo, M. Suzuki and Y. Shiratani, "Technology for production of High-Quality Slab at High-Speed Casting," *75 Steelmaking Conference Proceedings,* pp. 409–415, The Iron and Steel Society, 1992.
32. G-G. Lee, B.G. Thomas, S-H. Kim, H-J. Shin, S-K. Baek, C-H. Choi, D-S. Kim and S-J. Yu, "Microstructure Near Corners of Continuous-Cast Steel Slabs Showing Three-Dimensional Frozen Meniscus at Hooks," *Acta Materialia,* Vol. 55, No. 20, pp. 6705–6712, 2007.
33. J. Sengupta, B.G. Thomas, H-J. Shin, G-G. Lee and S-H. Kim, "A New Mechanism of Hook Formation During Continuous Casting of Ultralow-Carbon Steel Slabs," *Metallurgical and Materials Transactions A,* Vol. 37, No. 5, pp. 1597–1611, 2006.
34. S-M. Cho, G-G. Lee, S-H. Kim, R. Chaudhary, O-D. Kwon and B.G. Thomas, "Effect of Stopper-Rod Misalignment on Asymmetric Flow and Vortex Formation in Steel Slab Casting," *Proceedings of The Minerals, Metals, and Materials Society 139 Annual Meeting,* pp. 71–77, The Minerals, Metals and Materials Society, 2010.
35. N. Kasai and M. Iguchi, "Water-Model Experiment on Melting Powder Trapping by Vortex in the Continuous Casting Mold," *ISIJ International,* Vol. 47, No. 7, pp. 982–987, 2007.
36. B. Li, T. Okane and T. Umeda, "Modeling of Biased Flow Phenomena Associated With the Effects of Static Magnetic-Field Application and Argon Gas Injection in Slab Continuous Casting of Steel," *Metallurgical and Materials Transactions B,* Vol. 32, No. 6, pp. 1053–1066, 2001.
37. B. Li and F. Tsukihashi, "Vortexing Flow Patterns in a Water Model of Slab Continuous Casting Mold," *ISIJ International,* Vol. 45, No. 1, pp. 30–36, 2005.
38. Q. He, "Observations of Vortex Formation in the Mold of a Continuous Slab Caster," *ISIJ International,* Vol. 33, No. 2, pp. 343–345, 1993.
39. H. Bai and B.G. Thomas, "Effects of Clogging, Argon Injection, and Continuous Casting Conditions on Flow and Air Aspiration in Submerged Entry Nozzles," *Metallurgical and Materials Transactions B,* Vol. 32, No. 4, pp. 707–722, 2001.
40. S. Mahmood, "Efficient Modeling of Flow Asymmetries and Particle Entrapment in Nozzle and Mold During Continuous Casting of Steel Slabs," Master's thesis, University of Illinois at Urbana–Champaign, 2006.
41. L. Zhang, Y. Wang and X. Zuo, "Flow Transport and Inclusion Motion in Steel Continuous-Casting Mold Under Submerged Entry Nozzle Clogging Condition," *Metallurgical and Materials Transactions B,* Vol. 39, No. 4, pp. 534–550, 2008.
42. R. Chaudhary, G-G. Lee, B.G. Thomas, S-M. Cho, S-H. Kim and O-D. Kwon, "Effect of Stopper-Rod Misalignment on Fluid Flow in Continuous Casting of Steel," *Metallurgical and Materials Transactions B,* Vol. 42, pp. 300–315, 2011.
43. H. Bai and B.G. Thomas, "Turbulent Flow of Liquid Steel and Argon Bubbles in Slidegate Tundish Nozzles: Part I. Model Development and Validation," *Metallurgical and Materials Transactions B,* Vol. 32, No. 2, pp. 253–267, 2001.
44. H. Bai and B.G. Thomas, "Turbulent Flow of Liquid Steel and Argon Bubbles in Slidegate Tundish Nozzles: Part II. Effect of Operation Conditions and Nozzles Design," *Metallurgical and Materials Transactions B,* Vol. 32, No. 2, pp. 269–284, 2001.
45. M. Gebhard, Q. He and J. Herbertson, "Vortexing Phenomena in Continuous Slab Casting Molds," *76 Steelmaking Conference Proceedings,* pp. 441–446, The Iron and Steel Society, 1993.
46. B. Li and F. Tsukihashi, "Effects of Electromagnetic Brake on Vortex Flows in This Slab Continuous Casting Mold," *ISIJ International,* Vol. 46, No. 12, pp. 1833–1838, 2006.
47. G. Kastner, W. Brandstätter, B. Kaufmann, C. Wassermayr and M. Javurek, "Numerical Study on Mold Powder Entrapment Caused by Vortexing in a Continuous Casting Process," *Steel Research International,* Vol. 77, No. 6, pp. 404–408, 2006.
48. D. Gupta and A.K. Lahiri, "Cold Model Study of Slag Entrainment Into Liquid Steel in Continuous Slab Caster," *Ironmaking and Steelmaking,* Vol. 23, No. 4, pp. 361–363, 1996.
49. K. Tsutsumi, K. Watanabe, M. Suzuki, M. Nakada and T. Shiomi, "Effect of Properties of Mold Powder Entrapped in Molten Steel in a Continuous Casting Process," *VII International Conference on Molten Slags, Fluxes and Salts,* pp. 803–806, The South African Institute of Mining and Metallurgy, 2004.
50. K. Watanabe, K. Tsutsumi, M. Suzuki, M. Nakada and T. Shiomi, "Effect of Properties of Mold Powder Entrapped Into Molten Steel in a Continuous Casting Process," *ISIJ International,* Vol. 49, No. 8, pp. 1161–1166, 2009.
51. H.L.F. von Helmholtz, "Über discontinuierliche flueßigkeits-bewegungen," *Monatsberichte der Königlichen Preußische Akademie der Wissenschaften zu Berlin,* Vol. 23, pp. 215–228, 1868.
52. W. Thomson, "Hydrokinetic Solutions and Observations," *Philosophical Magazine,* Vol. 42, No. 281, pp. 362–377, 1871.
53. L.M. Milne-Thomson, *Theoretical Hydrodynamics,* 5 ed., Macmillan Press, London, U.K., 1968. Example XV.17.
54. M. Iguchi, J. Yoshida, T. Shimizu and Y. Mizuno, "Model Study on the Entrapment of Mold Powder Into Molten Steel," *ISIJ International,* Vol. 40, No. 7, pp. 685–691, 2000.
55. T. Funada and D.D. Joseph, "Viscous Potential Flow Analysis of Kelvin–Helmholtz Instability in a Channel," *Journal of Fluid Mechanics,* Vol. 445, pp. 263–283, 2001.
56. S. Chandrasekhar, *Hydrodynamic and Hydromagnetic Stability,* pp. 481–514, Clarendon Press, Oxford, U.K., 1961.
57. P-R. Cha and J-K. Yoon, "The Effect of a Uniform Direct Current Magnetic Field on the Stability of a Stratified Liquid Flux/Molten Steel System," *Metallurgical and Materials Transactions B,* Vol. 31, No. 2, pp. 317–326, 2000.
58. J.M. Harman and A.W. Cramb, "A Study of the Effect of Fluid Physical Properties Upon Droplet Emulsification," *79 Steelmaking Conference Proceedings,* pp. 773–784, The Iron and Steel Society, 1996.
59. W.H. Emling, T.A. Waugaman, S.L. Feldbauer and A.W. Cramb, "Subsurface Mold Slag Entrainment in Ultralow Carbon Steels," *77 Steelmaking Conference Proceedings,* pp. 371–379, The Iron and Steel Society, 1994.
60. S. Asai, "Fluid Flow and Mass Transfer in a Refining Process by Use of Stirring," *Proceedings of the 100 and 101 Nishiyama Memorial Lecture,* pp. 65–100, The Iron and Steel Institute of Japan, 1984.

61. H. Yuyama, S. Kashio, S. Tsuneoka, K. Ohtaki and N. Matsuda, "Development of Bath-Level Variation Detector in CC Mold," *Tetsu-to-Hagane,* Vol. 72, No. 12, p. S1018, 1986.

62. R. Hagemann, R. Schwarze, H.P. Heller and P.R. Scheller, "Model Investigations on the Stability of the Steel-Slag Interface in Continuous-Casting Process," *Metallurgical and Materials Transactions B,* Vol. 44, No. 1, pp. 80–90, 2013.

63. J. Savolainen, T. Fabritius and O. Mattila, "Effect of Fluid Physical Properties on the Emulsification," *ISIJ International,* Vol. 49, No. 1, pp. 29–36, 2009.

64. K. Krishnapisharody and G.A. Irons, "Modeling and Analysis of Slag Droplet Formation in Ladle Metallurgy Practice," *AISTech Conference Proceedings,* Vol. II, pp. 1243–1252, 2008.

65. K. Krishnapisharody and G.A. Irons, "Model Studies on Slag Droplet Generation in Gas-Stirred Ladles," *EPD Congress 2008, Proceedings of The Minerals, Metals, and Materials Society 138 Annual Meeting,* pp. 293–302, The Minerals, Metals, and Materials Society, 2008.

66. K. Krishnapisharody and G.A. Irons, "Numerical Simulation of Droplet Generation of the Buoyant Phase in Two-Phase Liquid Baths," *EPD Congress 2008, Proceedings of The Minerals, Metals, and Materials Society 138 Annual Meeting,* pp. 311–322, The Minerals, Metals, and Materials Society, 2008.

67. Z. Xiao, Y. Peng and C. Liu, "Modeling Study of the Entrapment Phenomena at the Slag-Metal Interface in the Gas-Stirred Ladle," *Chinese Journal of Metal Science and Technology,* Vol. 3, pp. 187–193, 1987.

68. T. Wei and F. Oeters, "A Model Test for Emulsion in Gas-Stirred Ladles," *Steel Research,* Vol. 63, No. 2, pp. 60–68, 1992.

69. B.G. Thomas, X. Huang and R.C. Sussman, "Simulation of Argon Gas Flow Effects in a Continuous Slab Caster," *Metallurgical and Materials Transactions B,* Vol. 25, No. 4, pp. 527–547, 1994.

70. J. Knoepke, M. Hubbard, J. Kelly, R. Kittridge and J. Lucas, "Pencil Blister Reduction at Inland Steel Company," *77 Steelmaking Conference Proceedings,* pp. 381–388, The Iron and Steel Society, 1994.

71. T. Watanabe and M. Iguchi, "Water Model Experiments on the Effect of an Argon Bubble on the Meniscus Near the Immersion Nozzle," *ISIJ International,* Vol. 49, No. 2, pp. 182–188, 2009.

72. S. Yamashita and M. Iguchi, "Mechanism of Mold Powder Entrapment Caused by Large Argon Bubble in Continuous Casting Mold," *ISIJ International,* Vol. 41, No. 12, pp. 1529–1531, 2001.

73. R.M. McDavid and B.G. Thomas, "Flow and Thermal Behavior of the Top Surface Flux/Powder Layers in Continuous Casting Molds," *Metallurgical and Materials Transactions B,* Vol. 27, No. 4, pp. 672–685, 1996.

74. B. Zhao, S.P. Vanka and B.G. Thomas, "Numerical Study of Flow and Heat Transfer in a Molten Flux Layer," *International Journal of Heat and Fluid Flow,* Vol. 26, No. 1, pp. 105–118, 2005.

75. J. Yoshida, T. Ohmi and M. Iguchi, "Cold Model Study on the Effects of Density Difference and Blockage Factor on Mold Powder Entrainment," *ISIJ International,* Vol. 45, No. 8, pp. 1160–1164, 2005.

76. Y. Ueda, T. Kida and M. Iguchi, "Unsteady Pressure Coefficient Around an Elliptic Immersion Nozzle," *ISIJ International,* Vol. 44, No. 8, pp. 1403–1409, 2004.

77. J.W. Rottman, "Steep Standing Waves at a Fluid Interface," *Journal of Fluid Mechanics,* Vol. 124, pp. 283–306, 1982.

78. W.G. Penney and A.T. Price, "Finite Periodic Stationary Gravity Waves in a Perfect Liquid," *Philosophical Transactions of the Royal Society of London A,* Vol. 244, No. 882, pp. 254–284, 1952.

79. L.W. Schwartz and A.K. Whitney, "A Semi-Analytic Solution for Nonlinear Standing Waves in Deep Water," *Journal of Fluid Mechanics,* Vol. 107, pp. 147–171, 1981.

80. A. Theodorakakos and G. Bergeles, "Numerical Investigation of the Interface in a Continuous Steel Casting Mold Water Model," *Metallurgical and Materials Transactions B,* Vol. 29, No. 6, pp. 1321–1327, 1998.

81. J. Anagnostopoulos and G. Bergeles, "Three-Dimensional Modeling of the Flow and the Interface Surface in a Continuous Casting Mold Model," *Metallurgical and Materials Transactions B,* Vol. 30, No. 6, pp. 1095–1105, 1999.

82. S.A. Thorpe, "On Standing Internal Gravity Waves of Finite Amplitude," *Journal of Fluid Mechanics,* Vol. 32, No. 3, pp. 489–528, 1968.

83. S.K. Dash, S.S. Mondal and S.K. Ajmani, "Mathematical Simulation of Surface Wave Created in a Mold Due to Submerged Entry Nozzle," *International Journal of Numerical Methods for Heat and Fluid Flow,* Vol. 14, No. 5, pp. 606–632, 2004.

84. D. Gupta and A.K. Lahiri, "Cold Model Study of the Surface Profile in a Continuous Slab Casting Mold: Effect of Second Phase," *Metallurgical and Materials Transactions B,* Vol. 27, No. 4, pp. 695–697, 1996.

85. F.M. Najjar, B.G. Thomas and D.E. Hershey, "Numerical Study of Steady Turbulent Flow Through Bifurcated Nozzles in Continuous Casting," *Metallurgical and Materials Transactions B,* Vol. 26, No. 4, pp. 749–765, 1995.

86. D. Gupta and A.K. Lahiri, "Water Modeling Study of the Jet Characteristics in a Continuous Casting Mold," *Steel Research,* Vol. 63, No. 5, pp. 201–204, 1992.

87. M. Kamal and Y. Sahai, "Modeling of Melt Flow and Surface Standing Waves in a Continuous Casting Mold," *Steel Research International,* Vol. 76, No. 1, pp. 44–52, 2005.

88. B. Rietow, "Fluid Velocity Simulation and Measurement in Thin-Slab Casting," Master's thesis, University of Illinois at Urbana–Champaign, 2007. ✦

This paper was presented at AISTech 2013 — The Iron & Steel Technology Conference and Exposition, Pittsburgh, Pa., and published in the Conference Proceedings.